Simen Owen Academic Proceedings Series

4th International Conference on Electronics, Engineering, Computer Science and Applied Development (EESD 2026)

Article

Material Selection and Structural Redesign of a 3D Printed Four Bar Mechanism for Prosthetic Joint Motion

Zijian Lin[1,*]

[1] International Department, Hefei 168 High School, Hefei, China
* Correspondence: Zijian Lin, International Department, Hefei 168 High School, Hefei, China

Abstract: Material selection for a printed joint mechanism depends on structural response, recovery and assembly conditions. This study combines an exploratory comparison of polylactic acid (PLA) and acrylonitrile butadiene styrene (ABS) specimens with the redesign of a four bar mechanism intended to demonstrate prosthetic joint motion. Fourteen distinct structural loading conditions and four spring conditions were analyzed at applied masses of 0.5 and 1.0 kg. Recorded displacement and uncalibrated voltage endpoints were retained separately. Apparent stiffness, paired displacement differences and origin constrained spring fits were calculated without treating loading levels as replicates. At 1.0 kg, the PLA plate and unrestrained double arch displaced 8.26 and 3.57 mm, respectively. ABS plate displacement exceeded PLA by 33.7%, whereas the corresponding difference for unrestrained arches was 10.4%. Fitted spring stiffness was 216.4 N/m for ABS and 380.9 N/m for PLA. ABS showed approximately 1 mm residual shortening, compared with 3–4 mm for PLA. A prototype combined ABS moving components, PLA supports, 4 mm interlink separation and shaft and pin location. Qualitative observations indicated smoother motion and no visible powder during the demonstration. The results support component level screening and assembly redesign; calibrated measurements, repeated tests and quantified wear remain necessary for prosthetic performance assessment.

Keywords: Additive manufacturing; Four bar linkage; Prosthetic joint prototype; Polymer component stiffness; Data guided material selection

1. Introduction

Joint mechanisms in a prosthetic limb must accommodate movement while transferring forces through connected components. A four-bar linkage offers a compact way to generate coupled rotation and translation using a small number of links. Its geometry determines the relative motion of the connected segments and the path of the instantaneous center of rotation. Established prosthetic-knee research relates these features to alignment and voluntary control of stability [1]. Broader reviews distinguish stance stability, early-stance flexion, and swing resistance as separate functional requirements [2]. These distinctions make four-bar mechanisms useful subjects for early engineering investigation, while also identifying the measurements needed as development progresses.

Three-dimensional printing provides an accessible route from a digital component model to an assembled mechanism. Designers can change plate profiles, link connections, and local clearances between fabrication cycles. Published reviews of printed upper-limb prostheses describe opportunities for geometric customization alongside incomplete reporting of functional performance and durability [3]. A systematic review also found that early studies commonly provided proof-of-concept evidence with limited clinical

Received: 06 September 2026
Revised: 20 October 2026
Accepted: 03 November 2026
Published: 07 November 2026

Copyright: © 2026 by the authors. Submitted for possible open access publication under the terms and conditions of the Creative Commons Attribution (CC BY) license (https://creativecommons.org/licenses/by/4.0/).

validation [4]. For a small printed joint prototype, the immediate engineering questions therefore concern assembly, deformation, recovery, and contact behavior. Answering these questions can guide subsequent structural testing and help define a suitable development scope.

Material selection is closely linked to component geometry and the printing process. Polylactic acid (PLA) and acrylonitrile butadiene styrene (ABS) are commonly available printing polymers, but their names alone do not determine the response of a finished part. Printed ABS can exhibit directional mechanical properties because its deposited filaments and interfaces form a structured material [5]. Comparisons of desktop-printed PLA and ABS also show that stiffness and strength depend on the fabrication conditions represented by the specimens [6]. A plate, arch, and spring made from one polymer can respond differently because their load paths, section shapes, and constraints differ. Material and topology consequently require joint consideration.

The distinction between immediate deformation and time-dependent recovery is particularly relevant when compliant components are introduced into a mechanism. A shape can return toward its initial position after unloading while retaining an offset over the observed interval. Short-term PLA investigations show that creep and recovery depend on manufacturing route, infill, and applied stress [7]. Fatigue studies address another timescale: repeated loading can accumulate damage through mechanisms that a single loading–unloading observation cannot quantify [8]. An exploratory comparison needs clearly defined endpoints and conservative interpretation of these different responses. Visible surface debris provides an additional reason to inspect the contact conditions around a moving joint.

The linkage geometry creates a further interaction between component behavior and assembly conditions. Four-bar analyses distinguish feasible motion intervals, turning points, and assembly circuits [9]. Prosthetic design studies extend the assessment to competing requirements such as stability, clearance, flexion, and the hip moment required for control [10]. At the prototype scale, changing a joint gap or replacing a connection can alter freedom of movement and load transfer even when the nominal link arrangement is retained. The resulting response must therefore be associated with the tested fixture and assembly configuration. Geometry-based motion predictions and physical component observations provide complementary information at this stage.

This study develops an experimental account of material selection and structural redesign for a printed four-bar mechanism intended to demonstrate prosthetic joint motion. The investigation includes PLA and ABS plates, arch and spring specimens, and an assembled prototype with 4 mm interlink separation and shaft–pin connections. Eighteen endpoint conditions form the basis of the quantitative comparison, with one observation available for each condition. The analysis organizes these observations by material, topology, and constraint arrangement. It separately examines deformation and recovery endpoints, the interpretation of spring stiffness, and the qualitative contact observations recorded during mechanism development.

The resulting contribution is a documented design progression supported by condition-specific measurements and explicit limits of inference. Printed prosthetic-socket research illustrates why structural results depend on fabrication, alignment, and reinforcement, and why values from other components cannot be transferred directly to a new design [11]. Evaluation of lower-limb technologies similarly distinguishes technical development, laboratory assessment, and field testing [12]. The present evidence belongs to the first of these stages. It supports selection of configurations for further investigation, clarifies the interaction between compliant topology and fixture conditions, and identifies the dimensional, cyclic-loading, and joint-contact measurements needed to assess a later prototype.

2. Related Work

2.1. Four Bar Mechanisms and Prosthetic Design Evaluation

Computational design of prosthetic four-bar mechanisms has a long history. Hobson and Torfason used computerized optimization to approximate specified centrodes for knee mechanisms [13]. This established a route from a desired motion description to linkage dimensions. Radcliffe subsequently explained how linkage geometry and alignment affect prosthetic-knee behavior [1]. Together, these studies show that choosing link lengths involves both a kinematic objective and a functional interpretation. A trajectory that can be generated by a linkage still requires assessment in the loading and alignment conditions of its intended application.

Mobility analysis addresses the motion permitted by an assembled mechanism. Bai developed a geometric treatment of coupler-link rotation, turning points, and circuits [9]. These distinctions are relevant when a physical model approaches a limiting configuration or follows one of several possible assembly branches. Anand and Sujatha used a wider set of geometric performance measures to compare polycentric knees, including stability, toe clearance, maximum flexion, and required hip moment [10]. Their approach illustrates the trade-offs between objectives and the additional gait measurements needed to assess a proposed geometry.

Several later investigations combine mechanical design with more specific forms of evaluation. Kapti and Yucenur implemented active joint-angle tracking in an artificial knee [14]. Wang and colleagues developed a printed, customizable knee using anatomical geometry, springs, and a flexible linkage; their evaluation examined how spring configuration influenced motion [15]. Phoengsongkhro and colleagues investigated stance-phase flexion in a four-bar knee through mechanism redesign and a single-subject pilot [16]. These studies use different topologies and levels of validation. They provide relevant design context without supplying performance evidence for a separate desktop assembly. The present work focuses on the preceding component-selection stage, where material response, compliant geometry, and connection details are being resolved.

2.2. Printed Polymer Mechanics and Structural Configuration

The response of a printed polymer component reflects both its constituent material and its deposited structure. Rodríguez, Thomas, and Renaud experimentally examined ABS produced by fused deposition and related its mechanical behavior to voids and processing effects [17]. Ahn and colleagues demonstrated directional properties in printed ABS [5]. These findings explain why a material label or a feedstock datasheet is insufficient for assigning stiffness or strength to a printed plate. They also motivate reporting the orientation of the deposited material relative to the applied load.

Process studies have examined several parameters simultaneously. Sood, Ohdar, and Mahapatra considered layer thickness, orientation, raster angle, raster width, and air gap in relation to mechanical performance [18]. Durgun and Ertan assessed orientation and raster angle alongside strength, surface finish, and production cost [19]. For PLA, Chacón and colleagues studied build orientation, layer thickness, and feed rate [20], while Lanzotti and colleagues examined layer thickness, infill direction, and shell-perimeter count [21]. The combined evidence supports controlled comparisons that retain fabrication conditions as part of the specimen description. Differences between materials should be interpreted within those conditions.

Interfilament bonding provides a physical explanation for some of this dependence. Bellehumeur and colleagues connected the formation of bonds between extruded filaments to thermal conditions and sintering behavior [22]. Sun and colleagues examined how processing conditions influence cooling, mesostructure, and bonding quality [23]. Coogan and Kazmer further distinguished bond strength from strength along the filament direction [24]. These studies concern the internal architecture of printed parts, whereas replacing a plate with an arch or spring changes the component-scale load path. Both scales contribute to measured displacement. A stiffness ratio between two spring configurations consequently describes the tested structures and constraints; identifying a polymer elastic modulus would additionally require a suitable material model, geometry,

and strain measurement. Published PLA–ABS comparisons are useful context [6], but they do not establish the properties of the present specimens.

2.3. Recovery Fatigue and Joint Contact Observations

Time-dependent deformation introduces requirements beyond a static displacement comparison. Gebrehiwot and colleagues measured short-term creep and recovery of tough PLA made through different fabrication routes [7]. Adibeig, Vakili-Tahami, and Saeimi-Sadigh investigated the influence of build direction and raster orientation on printed-PLA creep [25]. Such work relies on load and displacement histories to characterize evolution over time. Where a source record contains selected endpoints, the corresponding analysis can describe changes between those endpoints, while identification of a creep law or recovery timescale requires additional observations.

Fatigue performance also needs a loading protocol matched to the question. Afrose and colleagues found that the rankings of PLA build orientations under static and cyclic tensile testing were different under their tested conditions [26]. Safai and colleagues reviewed the influence of material, fabrication, and loading variables on printed-polymer fatigue [8]. These results caution against converting a favorable single-load displacement or recovery observation into a general durability ranking. A later joint assessment would need repeated specimens, specified cycle amplitudes and rates, and an operational definition of failure.

Contact behavior is similarly sensitive to the test configuration. Mohamed and colleagues investigated wear in printed polycarbonate–ABS blends [27]; their material system differs from neat ABS. Aziz, Ul Haq, and Raina showed that surface texture and operating conditions affect friction in printed PLA [28]. Accordingly, visible powder around a moving connection is a qualitative observation requiring follow-up measurement. It does not identify a wear rate, friction coefficient, or universal material ranking. The present prototype's connection changes can be discussed in terms of clearance and contact management. Establishing wear resistance would require defined contact loads, motion histories, counterface properties, and measurements of material loss or surface change. This separation keeps structural screening, recovery assessment, and tribological evaluation tied to their respective evidence.

3. Methodology

3.1. Study Design and Evidence Structure

The study links small specimen comparisons to a benchtop mechanism redesign. Its experimental starting point was a previously used plastic linkage that exhibited intermittent motion, lateral movement and visible white powder around contacting parts. These observations motivated separate comparisons of material, structural configuration and support restraint. The powder was treated as an observable indicator of surface interaction. Its composition and origin were not established by microscopy or chemical analysis. The resulting design question was how to reduce unintended contact while selecting components with suitable measured stiffness and post-loading shape retention.

Figure 1 summarizes the analysis workflow. Structural specimens were compared under two applied masses, and printed springs were examined for compression and residual shortening. The recorded observations were organized by material, geometry, restraint label and loading level. Repeated appearances of the same values in different comparison tables were consolidated before calculation. The component indicators were then related to the functions of moving links, connecting shafts, retaining pins and stationary supports. Prototype observations provide a separate qualitative outcome at the assembly level.

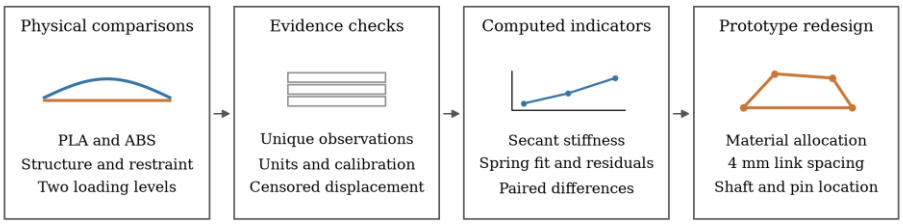


Figure 1. Workflow Linking Specimen Observations, Evidence Checks, Derived Component Indicators and Assembly Redesign. The Workflow Separates Measurement from Interpretation.

The experimental archive contains one observation for each documented condition. It does not establish the number of separately printed specimens or whether both loading levels were applied sequentially to the same specimen. Consequently, the observational unit is a load-condition record. The 0.5 and 1.0 kg measurements describe two loading levels and provide no estimate of between-specimen variation. The analysis retains this distinction throughout the tables, plots and interpretation. It reports measured endpoints, deterministic transformations of those endpoints and qualitative demonstration observations as separate forms of evidence.

Three comparisons guide the analysis. The first examines displacement in PLA truss, plate and double-arch specimens. The second compares PLA and ABS within a shared geometry and fixture label. The third examines changes associated with restraining both ends of an arch specimen. Spring measurements add a component-level stiffness and recovery comparison. These comparisons support local design decisions within the tested configurations. They do not constitute a factorial experiment capable of independently estimating all interactions among material, printing, geometry and boundary conditions.

3.2. Specimens and Measurement Chain

The specimens and mechanism parts were manufactured on a Bambu Lab P1S printer using fused deposition modeling (FDM). The structural specimens had a reported nominal length of 240 mm. The spring specimens had an initial length of 120 mm, with matching outer diameter, wire width and turn count specified qualitatively. The archived protocol describes matched printing settings for comparisons, but does not specify numerical layer height, infill fraction, raster orientation, shell count, extrusion temperature or bed temperature. These settings are therefore not assigned assumed values. The comparison is between the documented printed components, with manufacturing effects remaining part of their response.

The measurement equipment comprised BF350-1EB foil strain gauges, a direct-current excitation supply set to 3 V, a half-bridge arrangement, a Keithley 6514 electrometer and displacement measurements using a caliper. Applied masses were 500 and 1000 g. Loading was described as gradual, without intended impact. Table 1 records the conditions that can be carried into the analysis. Figure 2 reproduces an original photograph of the structural specimens. The photograph documents their broad form and does not replace dimensional drawings or an inspection of the internal printed structure.



Figure 2. Original Photograph of Printed Structural Specimens, Reproduced from the Experimental Project Record. The Visible Shapes Provide Context for the Topology Comparison; Nominal Specimen Length Is 240 Mm.

Table 1. Documented Measurement Conditions and Analysis Scope.

Item	Documented condition
Printer and polymers	Bambu Lab P1S; PLA and ABS
Structural specimen length	240 mm nominal; clear support span unspecified
Added test masses	0.5 and 1.0 kg; applied gradually
Spring initial length	120 mm; other dimensions matched qualitatively
Electrical measurement	BF350-1EB gauge; 3 V excitation; half bridge; Keithley 6514
Recorded increments	Voltage 0.001 V; numerical displacement 0.01 mm; truss reported <1 mm
Recorded observations	One observation per documented loading condition
Manufacturing metadata	Numerical print settings and material grades unavailable

The archive reports voltage differences to 0.001 V and most displacement values to 0.01 mm. These are recording increments, not validated measurement uncertainties. The truss displacement was recorded only as less than 1 mm. That threshold is retained as a censored observation despite the finer nominal caliper increment specified elsewhere. Temperature and humidity targets were listed, but numerical environmental observations were not retained with the measurement table. Actual environmental stability is consequently not used as an established control variable.

Voltage endpoints represent instrument-output changes between baseline and loaded states. Gauge factor, bridge-arm configuration, amplifier gain and an end-to-end strain calibration were not established. The voltage values remain in their recorded unit of volts and are not converted to strain, stress or elastic modulus. High-rate acquisition and filtering descriptions cannot be resolved from the endpoint archive, so the analysis does not estimate frequency response, transient settling time or spectral features. The displacement channel supplies the dimensional basis for apparent stiffness, while the voltage channel provides an additional descriptive response to loading.

3.3. Endpoint Calculations and Component Indicators

Applied force F was calculated from added mass m using conventional standard gravity g = 9.80665 m/s^2. Equation (1) gives the conversion. The two loading levels correspond to 4.903325 and 9.806650 N. Calculations use these unrounded values; tables show 4.90 and 9.81 N where appropriate. The calculation represents the added test load. Specimen self-weight and any fixture contribution cannot be incorporated into an absolute internal-force model because their load paths and zeroing procedure were not specified.

$$F = mg \quad \textbf{(1)}$$

The voltage endpoint is defined in Eq. (2), where V_{load} and V_{base} denote the loaded and unloaded steady-state readings, respectively. This equation describes the recorded feature, without assuming an averaging procedure or generating new samples from waveform screenshots. An additive offset common to both readings would cancel, while time-dependent drift could remain. Each tabulated voltage is consequently treated as a measured feature whose calibration and uncertainty require separate assessment.

$$\Delta V = V_{load} - V_{base} \quad \textbf{(2)}$$

For a structural specimen, the apparent secant stiffness K is the applied force divided by the recorded vertical displacement Δh, as shown in Eq. (3). Structural calculations use millimeters and report K in N/mm. For springs, the same force-to-displacement construction uses compression Δx expressed in meters and reports stiffness k in N/m. K and k describe complete components under their respective loading arrangements. Geometry, interfaces and fixture movement contribute to these quantities, which are distinct from a material elastic modulus.

$$K = \frac{F}{\Delta h}, \quad k = \frac{F}{\Delta x} \quad \textbf{(3)}$$

Paired differences are reported with an explicit reference condition. Equation (4) defines percentage change P for a response a relative to a reference b. Material displacement differences use PLA as b; restraint differences use the unrestrained state as b. A displacement reduction of the arch relative to the plate is stated with the plate as the denominator. No percentages combine different physical units. Truss displacement remains an upper bound, so the corresponding stiffness is a lower bound under the positive-displacement interpretation of the measurement.

$$P(a,b) = 100\,(\frac{a}{b} - 1)\,\% \quad \textbf{(4)}$$

For each spring material, a retrospective origin-constrained least-squares fit summarizes the two loading endpoints. Equation (5) estimates k_0 by minimizing squared force residuals, with index i covering the two observed conditions and $x_i = \Delta x_i$ representing measured compression in meters. The origin is a model constraint, not an additional measured point. Residuals ei are defined in Eq. (6). The fit is used for a descriptive comparison of component response over the measured loading interval; no goodness-of-fit statistic is interpreted as independent validation.

$$k_0 = \frac{\sum_{i=1}^{2} x_i F_i}{\sum_{i=1}^{2} x_i^2} \quad \textbf{(5)}$$

$$e_i = F_i - k_0 x_i \quad (6)$$

After-test shortening is expressed as a percentage r of initial spring length using Eq. (7). Here Li is the initial length and L_s is the reported post-test length. The record gives approximate final lengths for each material without pairing them unambiguously to individual loads or specifying the recovery delay. The analysis therefore reports residual-length percentages and does not calculate a percentage recovery of maximum compression. Time-dependent recovery and permanent set cannot be separated from these observations.

$$r = 100\,\frac{L_i - L_p}{L_i}\,\% \quad \textbf{(7)}$$

3.4. Linkage Representation and Assembly Redesign

The mechanism is represented as a planar four bar linkage with ground pivots O and D, moving pivots A and B, and four link lengths l_0 through l_3. The ground link OD defines the horizontal reference. Link OA has length l_1 and angle θ_1; AB has length l_2 and angle θ_2; DB has length l_3 and angle θ_3. Angles are measured from the same positive horizontal axis. Equations (8) and (9) express the horizontal and vertical loop closure. They identify the geometric quantities required for a subsequent motion analysis.

$$l_1 \cos\theta_1 + l_2 \cos\theta_2 = l_0 + l_3 \cos\theta_3 \quad \textbf{(8)}$$

$$l_1 \sin\theta_1 + l_2 \sin\theta_2 = l_3 \sin\theta_3 \quad (9)$$

The symbolic diagram in Figure 3 defines this notation. Its drawn proportions are illustrative and are not measurements of the prototype. The experimental archive does not provide the four link lengths, pivot coordinates or an input-angle trajectory. No numerical kinematic optimization, transmission-angle curve or human-joint trajectory fit is therefore attributed to the present study. A numerical reconstruction would require those geometric inputs and a specified assembly branch before output motion could be calculated consistently.

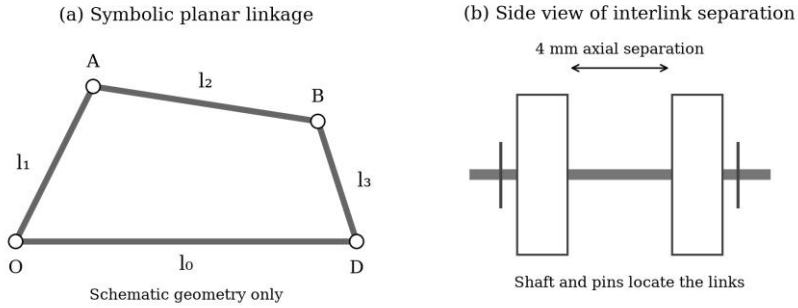


Figure 3. Symbolic Four Bar Geometry and Interlink Separation. Panel (a) Defines the Links and Pivots in Eqs. (8) and (9); Drawn Proportions Are Not Prototype Dimensions. Panel (B) Illustrates the Reported 4 Mm Axial Separation, Distinct from Radial Bearing Clearance.

The implemented redesign combined several changes. Adjacent moving links were arranged in parallel with a reported 4 mm separation, and shafts and pins were used for location. This dimension describes axial separation between neighboring links; it is not a radial pin-hole clearance. Sleeve-to-shaft fit and the distribution of contacting surfaces were also revised. Their intended mechanical role was to reduce unwanted side-face rubbing and uncontrolled lateral displacement while maintaining the designed rotational motion. Bearing fit tolerances and contact pressures were not measured.

ABS was assigned to moving links, shafts and pins, while PLA was retained for stationary supports and the base. This allocation used the component comparisons as screening evidence, supplemented by the different functional requirements of moving and stationary parts. Spring recovery does not directly measure pin shear strength or shaft wear. Those component choices remain candidates for subsequent targeted tests. The prototype evaluation recorded whether motion appeared continuous, whether lateral movement remained visible and whether fresh powder was visible during the demonstration.

3.5. Data Handling and Interpretation Rules

The numerical analysis preserves all documented endpoints without imputation, outlier removal or invented repeated runs. Units and fixture labels accompany every comparison. Four repeated entries, corresponding to the two PLA plate and two unrestrained PLA arch conditions, are counted once when establishing the dataset size. The resulting dataset contains fourteen structural endpoints and four spring endpoints. The structural comparison plots connect the two observed masses only to aid reading; connecting lines do not indicate additional measured loading conditions.

All percentages, stiffness estimates and fit residuals are calculated directly from the transcribed measurements using deterministic arithmetic. Display rounding is applied after computation. No standard deviation, confidence interval or significance test is reported because independent repeats are unavailable. Interpretation proceeds from a measured comparison to a component-level implication and then to the additional test needed for a design decision. This prevents a qualitative demonstration from acquiring the evidential status of a quantified wear, fatigue or clinical evaluation.

4. Experiments and Results

4.1. Structural Endpoints and Data Completeness

Table 2 consolidates the fourteen distinct structural records. Every structural measurement used one of the two added masses and a specimen with a nominal length of 240 mm. The longest recorded displacement was 11.04 mm for the unrestrained ABS plate under 1.0 kg. The smallest numerical displacement was 1.86 mm for the unrestrained PLA double arch under 0.5 kg. The PLA truss remained below its reported 1 mm threshold at both loads. These censored results are listed separately from the numerical range and are not entered into averages as zero values.

Table 2. Distinct Structural Endpoints and Derived Apparent Stiffness. U Denotes Unrestrained Placement; R Denotes Two-End Restraint; T Denotes the Topology Test with No Further Fixture Specification. Values Below 1 Mm Remain Censored.

Material	Shape	Fixture	Mass (kg)	ΔV (V)	Δh (mm)	K (N/mm)
PLA	Truss	T	0.5	0.046	<1	>4.90
PLA	Truss	T	1.0	0.082	<1	>9.81
PLA	Plate	U	0.5	0.163	4.32	1.135
PLA	Plate	U	1.0	0.389	8.26	1.187
ABS	Plate	U	0.5	0.207	5.13	0.956
ABS	Plate	U	1.0	0.418	11.04	0.888
PLA	Arch	U	0.5	0.118	1.86	2.636
PLA	Arch	U	1.0	0.211	3.57	2.747
PLA	Arch	R	0.5	0.172	2.17	2.260
PLA	Arch	R	1.0	0.247	4.03	2.433
ABS	Arch	U	0.5	0.204	2.06	2.380
ABS	Arch	U	1.0	0.338	3.94	2.489
ABS	Arch	R	0.5	0.286	2.92	1.679
ABS	Arch	R	1.0	0.413	4.21	2.329

Across structural conditions, recorded voltage differences span 0.046–0.418 V. Expressed in millivolts, this is 46–418 mV. The recording increment of 0.001 V corresponds to 1 mV. Retaining this scale avoids conflating instrument sensitivity with the magnitude of the recorded response. Each structural configuration shows a larger voltage difference at the higher load. That ordering is compatible with increased mechanical response, but a common conversion coefficient across materials or specimen shapes cannot be established from the available measurements.

The consolidated table also makes data reuse explicit. The PLA plate observations appear in both the topology and material comparisons, and the unrestrained PLA arch observations appear in both the topology and restraint comparisons. They provide shared reference conditions, not repeated experimental confirmation. A larger table count would overstate the number of independent observations. The spring records add four loading endpoints, while the approximate post-test lengths provide a separate, less precisely specified observation for each material.

4.2. Structural Configuration Comparison

For the PLA specimens at 0.5 kg, recorded vertical displacement was 4.32 mm in the plate and 1.86 mm in the unrestrained double arch. At 1.0 kg, the corresponding values were 8.26 and 3.57 mm. Relative to the plate, the arch displacement was 56.9% lower at 0.5 kg and 56.8% lower at 1.0 kg. The agreement of these percentages describes the two measured conditions. It does not establish their uncertainty or guarantee the same reduction under a different support arrangement.

The calculated apparent stiffness of the PLA plate was 1.135 N/mm at the lower load and 1.187 N/mm at the higher load. The corresponding unrestrained arch values were 2.636 and 2.747 N/mm. This approximately 2.3-fold difference concerns the tested structural assemblies. A material-modulus comparison would additionally require cross-

sectional geometry, an appropriate mechanical model and a defined support span. Nominal specimen length alone is insufficient for that conversion.

The truss displacement values support only bounded comparisons. Under the positive-displacement interpretation, a displacement below 1 mm gives apparent stiffness greater than 4.90 N/mm at 0.5 kg and greater than 9.81 N/mm at 1.0 kg. These bounds indicate less observed movement than in the other PLA configurations at the same added loads. They do not quantify a stiffness ratio between the two truss loading states because both denominators are censored.

A load path with substantial axial action is a plausible explanation for the small truss displacement, while arch geometry can redistribute bending and axial forces. The printed specimens are monolithic structures with finite joint stiffness, so ideal pin-jointed truss assumptions cannot be taken as experimentally verified. Their masses and effective section properties were not fully characterized. The measurements support a displacement ranking for the tested pieces, while strength, buckling resistance and stiffness per unit mass require additional information.

4.3. Material and Restraint Effects

Figure 4 compares the numerical displacement observations using the same vertical scale across three configurations. In panel (a), the unrestrained ABS plate displaced 5.13 mm at 0.5 kg and 11.04 mm at 1.0 kg, compared with 4.32 and 8.26 mm for PLA. Relative to PLA, ABS displacement was 18.8% higher at the lower load and 33.7% higher at the higher load. Its apparent stiffness changed from 0.956 to 0.888 N/mm. The two-point loading response therefore differs from that of the PLA plate, whose secant stiffness increased slightly over the same interval.

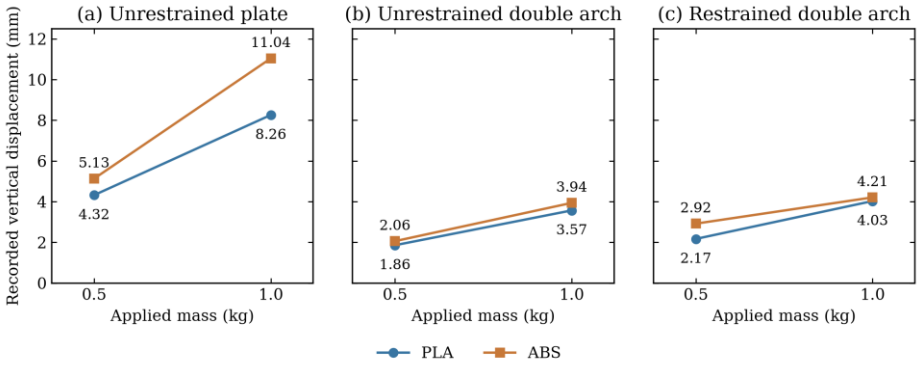


Figure 4. Recorded Displacement at 0.5 and 1.0 Kg for (a) Unrestrained Plates, (B) Unrestrained Double Arches and (C) Two-End-Restrained Double Arches. Lines Connect the Two Reported Endpoints Only. The Truss Is Omitted Because Its Displacement Was Recorded Only as Less Than 1 Mm. Independent Repeats Are Unavailable.

For the unrestrained arches in panel (b), ABS displaced 2.06 and 3.94 mm, compared with PLA values of 1.86 and 3.57 mm. The material differences were 10.8% and 10.4%, respectively. At 1.0 kg, comparing 33.7% for plates with 10.4% for unrestrained arches preserves the common fixture label. This suggests that the material contrast depends on the structural arrangement. It does not isolate topology as the sole cause because cross sections, contact details and print architecture also affect the measured response.

Panel (c) shows the two-end-restrained arch observations. At 0.5 kg, displacement was 2.92 mm for ABS and 2.17 mm for PLA, a 34.6% difference relative to PLA. At 1.0 kg, the values were 4.21 and 4.03 mm, a 4.5% difference. The material contrast changes with loading level under this restraint label. A single percentage would conceal that dependence. In particular, the 4.5% difference cannot serve as a general description of the arch material comparison.

Table 3 examines restraint within each material. The restrained PLA arch displaced 16.7% more than the unrestrained PLA arch at 0.5 kg and 12.9% more at 1.0 kg. For ABS,

the corresponding increases were 41.7% and 6.9%. Recorded voltage differences also increased following restraint. Thus, the observed direction of displacement change is consistently positive, although its magnitude varies. These measurements cannot support a statement that fixing both ends increased the apparent rigidity of the tested arrangement.

Table 3. Change in Recorded Arch Displacement with Restraint, Using the Unrestrained State as the Reference.

Material	Mass (kg)	Unrestrained (mm)	Restrained (mm)	Change (%)
PLA	0.5	1.86	2.17	+16.7
PLA	1.0	3.57	4.03	+12.9
ABS	0.5	2.06	2.92	+41.7
ABS	1.0	3.94	4.21	+6.9

The restrained and unrestrained configurations are fixture descriptions, with insufficient geometric information to impose ideal beam boundary conditions. Changes in support contact, specimen seating or the displacement reference could alter the recorded movement. These are possible explanations, not measured causes. The observation motivates better fixture metrology before using boundary conditions as a design rule. In the mechanism, reliable axial location remains a distinct assembly objective; the arch tests alone do not prove that a particular pinning scheme minimizes deformation.

The reported double-arch masses were 46.4 g for ABS and 60.1 g for PLA. ABS was therefore 22.8% lighter relative to the PLA specimen. This difference cannot be used to remove manufacturing effects from the material comparison. It may reflect polymer density, printed internal structure, dimensions or their combination. Weight reduction and stiffness would require a jointly documented geometry and manufacturing record before they could be evaluated as a normalized design objective.

4.4. Spring Compression and Residual Shortening

Table 4 lists the four spring endpoints and their derived secant stiffness. Under 0.5 kg, the ABS spring compressed by 23.00 mm and the PLA spring by 13.00 mm. Under 1.0 kg, the respective compressions were 45.14 and 25.68 mm. Using the common applied forces, ABS secant stiffness was 213.2 and 217.2 N/m, while PLA stiffness was 377.2 and 381.9 N/m. The PLA-to-ABS stiffness ratios were 1.769 and 1.758 at the lower and higher loading levels.

Table 4. Spring Compression and Secant Stiffness. Applied Force Is Calculated from Added Mass. Post-test Length Was Approximately 119 Mm for ABS and 116–117 Mm for PLA, from an Initial Length of 120 Mm; These Final Lengths Are Not Assigned to Individual Loads.

Material	Mass (kg)	Force (N)	Δx (mm)	k (N/m)
ABS	0.5	4.90	23.00	213.2
ABS	1.0	9.81	45.14	217.2
PLA	0.5	4.90	13.00	377.2
PLA	1.0	9.81	25.68	381.9

Figure 5(a) shows the two measured points for each material and the origin-constrained fits. The fitted stiffness was 216.4 N/m for ABS and 380.9 N/m for PLA, giving a ratio of 1.760. The signed force residuals for ABS were −0.074 and +0.038 N in increasing-load order. For PLA they were −0.049 and +0.025 N. Relative to the applied force at each point, the largest absolute residual was 1.51% for ABS and 0.99% for PLA. These residuals describe the fit to the same observations used to estimate its slope.

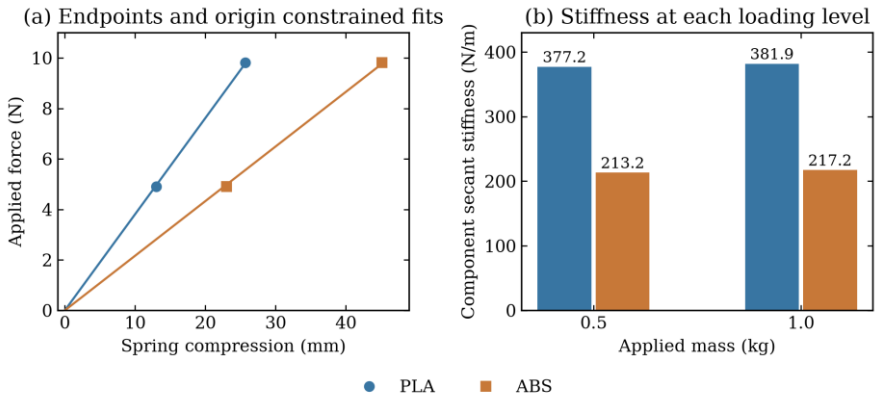


Figure 5. Spring Loading Response. Panel (a) Shows Measured Endpoints and Retrospective Origin-Constrained Fits; the Origin Is Not a Third Measured Observation. Panel (B) Shows Secant Stiffness at Each Loading Level. No Replicate-Based Error Bars Are Available.

Figure 5(b) presents stiffness at each loading level. The increase from the lower-load secant estimate to the higher-load estimate was 1.91% for ABS and 1.25% for PLA. The two estimates are therefore close within each material under these particular conditions. However, a two-level loading comparison cannot establish a constant constitutive stiffness over a broad range. The fit also supplies no measurement of unloading hysteresis. Its practical role is to summarize the observed loading response in a form that can be compared across the two printed springs.

Post-test length was approximately 119 mm for ABS and 116–117 mm for PLA, against an initial length of 120 mm. The corresponding residual shortening was approximately 1 mm and 3–4 mm. Normalizing by initial length gives approximately 0.83% for ABS and 2.50–3.33% for PLA. These values are residual-length fractions, not percentages of elastic recovery. Recovery delay, peak-load pairing and unloading rate were unspecified, so permanent deformation cannot be separated from delayed recovery or measurement effects.

The spring comparison exposes a design trade-off: the tested PLA spring resisted compression more strongly, while ABS retained a length closer to its initial value after the reported test sequence. A mechanism requiring position retention may value these attributes differently from one requiring compliant motion. The measured ratio applies to the complete spring geometry and printing conditions. It should not be transferred directly to the elastic modulus, fatigue life or friction properties of a shaft, pin or linkage member.

4.5. Assembly Observations and Design Implications

Figure 6 shows the printed mechanism in the benchtop demonstration. The implemented configuration used ABS for moving components and PLA for stationary components. Its redesign also introduced the reported 4 mm interlink separation, parallel arrangement and shaft and pin location. Table 5 relates these changes to their component functions and the available evidence. Separating contacting link faces can remove an unintended rubbing interface, while axial location can limit lateral motion. These assembly changes are directly connected to the initial observations of rubbing and wobble.

Table 5. Implemented Component Choices and Their Evidential Scope.

Component or feature	Implemented choice	Relevant evidence and outstanding test
Moving links	ABS	Smaller spring residual shortening; link cyclic strength untested
Shafts and retaining pins	ABS with axial location	Assembly observation; bearing wear and pin shear untested

Stationary supports and base	PLA	Higher stiffness in tested comparisons; assembly load capacity untested
Adjacent links	4 mm axial separation; parallel arrangement	Qualitative reduction of rubbing symptoms; torque and wear unmeasured



Figure 6. Original Photograph of the Benchtop Four Bar Mechanism Demonstration, Reproduced from the Project Record. The Image Documents the Assembly; Motion, Operating Duration and Wear Cannot Be Quantified from a Single Frame.

During the reported demonstration, motion appeared more continuous, lateral movement was reduced and no fresh white powder was visibly observed. These are qualitative observations of the assembled prototype. The observation duration, operating cycles, drive speed and applied joint torque were not quantified. Consequently, no percentage reduction in friction, wear rate or power loss is assigned. The photograph documents the apparatus and cannot independently demonstrate the motion sequence described in the experimental record.

Several changes were implemented together, which prevents attribution of the observed improvement to a single material or geometric feature. A reduction in visible powder could result from eliminating face contact, improving alignment, changing contact materials or a combination of these effects. The evidence supports retaining the revised arrangement as a candidate design for instrumented testing. It does not rank the separate changes by effectiveness.

The quantitative specimen results and qualitative prototype observations address different questions. The former show how the tested components responded to small added loads. The latter indicate that the assembled mechanism could move with fewer visible symptoms during demonstration. Their combination provides a traceable basis for the next design iteration, while component shear strength, bearing pressure, wear accumulation and physiological-load performance remain separate evaluation tasks.

5. Discussion

The central finding is that component choice changes when stiffness, residual shortening and assembly behavior are considered together. PLA showed lower displacement in the paired structural comparisons and higher spring stiffness. ABS showed smaller reported post-test spring shortening. This supports a function-dependent screening approach. A rigid support and a moving connection may require different balances, even when both are printed on the same machine. The measured evidence is strongest for the specific tested components and weakest for unmeasured properties such as pin fatigue and sliding wear.

The restraint result is particularly important for interpretation. Every restrained arch observation had a larger recorded displacement than its unrestrained counterpart. Treating restraint as automatically beneficial would reverse the direction of the measurements. A defined reference frame, measured support movement and a repeatable contact arrangement are needed to distinguish structural deformation from fixture effects. The small dataset makes these measurement definitions more consequential, because variation cannot be averaged over repeated independent specimens.

The redesign addressed unwanted rubbing through interlink separation and location, but nominal contact area alone cannot determine polymer friction. Contact pressure, surface texture, sliding speed and material pairing also matter [28]. A shorter post-test spring length likewise requires a timed recovery record before permanent set can be identified. The distinction between short-term shape retention and service fatigue follows the separate experimental requirements documented in printed-polymer fatigue research [8].

The next evaluation should first reproduce the specimen comparisons with identified print settings, calibrated force and displacement channels, and independent specimens. The voltage chain requires a documented bridge configuration and an end-to-end calibration. A subsequent assembly study should vary material allocation, interlink separation and axial location independently while measuring torque, angular play and wear over stated cycles. Link dimensions and measured trajectories are needed before comparing the mechanism with a target prosthetic motion. Human-use conclusions would require further structural and functional evaluation under appropriate oversight. The current study establishes an exploratory design case and a set of testable component choices, with no clinical performance claim.

6. Conclusion

This study examined printed polymer components and applied the observations to a four bar mechanism for demonstrating prosthetic joint motion. The analysis consolidated fourteen structural load-condition records and four spring records, preserving the distinction between numerical endpoints, censored displacements and qualitative prototype observations. Apparent stiffness and paired percentage changes provided component-level measures without converting uncalibrated voltage signals into material properties.

The tested unrestrained PLA double arch displaced approximately 57% less than the PLA plate at both loading levels. Under the common unrestrained fixture label at 1.0 kg, ABS displacement exceeded PLA by 33.7% for plates and 10.4% for arches. Restraining the arches increased recorded displacement in every paired comparison, demonstrating the need to characterize the fixture and measurement reference before assigning a stiffness benefit to restraint. The truss remained below the reported 1 mm displacement threshold, which supports bounded comparisons only.

The origin-constrained spring fits gave stiffness values of 216.4 N/m for ABS and 380.9 N/m for PLA. Their ratio of 1.760 describes the tested springs. Approximate residual shortening was 1 mm for ABS and 3–4 mm for PLA, indicating a different balance between loading stiffness and post-test shape retention. Recovery timing and independent repetitions are needed to establish the persistence and variability of that difference.

The prototype combined ABS moving components, PLA stationary supports, 4 mm interlink separation and shaft and pin location. The reported demonstration showed smoother motion and no visible fresh powder, providing qualitative support for further evaluation of the combined redesign. The available evidence does not quantify friction, wear life or safe prosthetic loading. Documented manufacturing conditions, calibrated measurements, repeated component tests and instrumented linkage evaluation are the next requirements for developing this benchtop concept into a characterized mechanism. The resulting design approach keeps measured component behavior connected to specific assembly decisions and to the evidence needed for their verification.

References

1. C. W. Radcliffe, "Four-bar linkage prosthetic knee mechanisms: Kinematics, alignment and prescription criteria," *Prosthetics and Orthotics International*, vol. 18, no. 3, pp. 159–173, 1994, doi: 10.3109/03093649409164401.
2. W. Liang, Z. Qian, W. Chen, H. Song, Y. Cao, G. Wei, L. Ren, K. Wang, and L. Ren, "Mechanisms and component design of prosthetic knees: A review from a biomechanical function perspective," *Frontiers in Bioengineering and Biotechnology*, vol. 10, Art. no. 950110, 2022, doi: 10.3389/fbioe.2022.950110.
3. J. ten Kate, G. Smit, and P. Breedveld, "3D-printed upper limb prostheses: A review," *Disability and Rehabilitation: Assistive Technology*, vol. 12, no. 3, pp. 300–314, 2017, doi: 10.1080/17483107.2016.1253117.
4. L. E. Diment, M. S. Thompson, and J. H. M. Bergmann, "Three-dimensional printed upper-limb prostheses lack randomised controlled trials: A systematic review," *Prosthetics and Orthotics International*, vol. 42, no. 1, pp. 7–13, 2018, doi: 10.1177/0309364617704803.
5. S.-H. Ahn, M. Montero, D. Odell, S. Roundy, and P. K. Wright, "Anisotropic material properties of fused deposition modeling ABS," *Rapid Prototyping Journal*, vol. 8, no. 4, pp. 248–257, 2002, doi: 10.1108/13552540210441166.
6. B. M. Tymrak, M. Kreiger, and J. M. Pearce, "Mechanical properties of components fabricated with open-source 3-D printers under realistic environmental conditions," *Materials & Design*, vol. 58, pp. 242–246, 2014, doi: 10.1016/j.matdes.2014.02.038.
7. S. Z. Gebrehiwot, L. Espinosa-Leal, M. Andersson, and H. Remes, "On the short-term creep and recovery behaviors of injection molded and additive-manufactured tough polylactic acid polymer," *Journal of Materials Engineering and Performance*, vol. 32, no. 22, pp. 10412–10430, 2023, doi: 10.1007/s11665-023-08278-6.
8. L. Safai, J. S. Cuellar, G. Smit, and A. A. Zadpoor, "A review of the fatigue behavior of 3D printed polymers," *Additive Manufacturing*, vol. 28, pp. 87–97, 2019, doi: 10.1016/j.addma.2019.03.023.
9. S. Bai, "Geometric analysis of coupler-link mobility and circuits for planar four-bar linkages," *Mechanism and Machine Theory*, vol. 118, pp. 53–64, 2017, doi: 10.1016/j.mechmachtheory.2017.07.019.
10. T. S. Anand and S. Sujatha, "A method for performance comparison of polycentric knees and its application to the design of a knee for developing countries," *Prosthetics and Orthotics International*, vol. 41, no. 4, pp. 402–411, 2017, doi: 10.1177/0309364616652017.
11. S. Kim, S. Yalla, S. Shetty, and N. J. Rosenblatt, "3D printed transtibial prosthetic sockets: A systematic review," *PLOS ONE*, vol. 17, no. 10, Art. no. e0275161, 2022, doi: 10.1371/journal.pone.0275161.
12. J. Andrysek, "Lower-limb prosthetic technologies in the developing world: A review of literature from 1994–2010," *Prosthetics and Orthotics International*, vol. 34, no. 4, pp. 378–398, 2010, doi: 10.3109/03093646.2010.520060.
13. D. A. Hobson and L. E. Torfason, "Optimization of four-bar knee mechanisms—A computerized approach," *Journal of Biomechanics*, vol. 7, no. 4, pp. 371–376, 1974, doi: 10.1016/0021-9290(74)90032-3.
14. A. O. Kapti and M. S. Yucenur, "Design and control of an active artificial knee joint," *Mechanism and Machine Theory*, vol. 41, no. 12, pp. 1477–1485, 2006, doi: 10.1016/j.mechmachtheory.2006.01.017.
15. K. Wang, H. Williams, Z. Qian, G. Wei, H. Xiu, W. Chen, X. Lu, J. Jin, L. Ren, W. Liang, and L. Ren, "Design and evaluation of a smooth-locking-based customizable prosthetic knee joint," *Journal of Mechanisms and Robotics*, vol. 16, no. 4, Art. no. 041008, 2024, doi: 10.1115/1.4062498.
16. S. Phoengsongkhro, P. Tangpornprasert, P. Yotnuengnit, M. Samala, and C. Virulsri, "Development of four-bar polycentric knee joint with stance-phase knee flexion," *Scientific Reports*, vol. 13, Art. no. 22809, 2023, doi: 10.1038/s41598-023-49879-4.
17. J. F. Rodríguez, J. P. Thomas, and J. E. Renaud, "Mechanical behavior of acrylonitrile butadiene styrene (ABS) fused deposition materials. Experimental investigation," *Rapid Prototyping Journal*, vol. 7, no. 3, pp. 148–158, 2001, doi: 10.1108/13552540110395547.
18. A. K. Sood, R. K. Ohdar, and S. S. Mahapatra, "Parametric appraisal of mechanical property of fused deposition modelling processed parts," *Materials & Design*, vol. 31, no. 1, pp. 287–295, 2010, doi: 10.1016/j.matdes.2009.06.016.
19. I. Durgun and R. Ertan, "Experimental investigation of FDM process for improvement of mechanical properties and production cost," *Rapid Prototyping Journal*, vol. 20, no. 3, pp. 228–235, 2014, doi: 10.1108/RPJ-10-2012-0091.
20. J. M. Chacón, M. A. Caminero, E. García-Plaza, and P. J. Núñez, "Additive manufacturing of PLA structures using fused deposition modelling: Effect of process parameters on mechanical properties and their optimal selection," *Materials & Design*, vol. 124, pp. 143–157, 2017, doi: 10.1016/j.matdes.2017.03.065.

21. A. Lanzotti, M. Grasso, G. Staiano, and M. Martorelli, "The impact of process parameters on mechanical properties of parts fabricated in PLA with an open-source 3-D printer," *Rapid Prototyping Journal*, vol. 21, no. 5, pp. 604–617, 2015, doi: 10.1108/RPJ-09-2014-0135.
22. C. Bellehumeur, L. Li, Q. Sun, and P. Gu, "Modeling of bond formation between polymer filaments in the fused deposition modeling process," *Journal of Manufacturing Processes*, vol. 6, no. 2, pp. 170–178, 2004, doi: 10.1016/S1526-6125(04)70071-7.
23. Q. Sun, G. M. Rizvi, C. T. Bellehumeur, and P. Gu, "Effect of processing conditions on the bonding quality of FDM polymer filaments," *Rapid Prototyping Journal*, vol. 14, no. 2, pp. 72–80, 2008, doi: 10.1108/13552540810862028.
24. T. J. Coogan and D. O. Kazmer, "Bond and part strength in fused deposition modeling," *Rapid Prototyping Journal*, vol. 23, no. 2, pp. 414–422, 2017, doi: 10.1108/RPJ-03-2016-0050.
25. M. R. Adibeig, F. Vakili-Tahami, and M.-A. Saeimi-Sadigh, "Numerical and experimental investigation on creep response of 3D printed Polylactic acid (PLA) samples. Part I: The effect of building direction and unidirectional raster orientation," *Journal of the Mechanical Behavior of Biomedical Materials*, vol. 145, Art. no. 106025, 2023, doi: 10.1016/j.jmbbm.2023.106025.
26. M. F. Afrose, S. H. Masood, P. Iovenitti, M. Nikzad, and I. Sbarski, "Effects of part build orientations on fatigue behaviour of FDM-processed PLA material," *Progress in Additive Manufacturing*, vol. 1, nos. 1–2, pp. 21–28, 2016, doi: 10.1007/s40964-015-0002-3.
27. O. A. Mohamed, S. H. Masood, J. L. Bhowmik, and A. E. Somers, "Investigation on the tribological behavior and wear mechanism of parts processed by fused deposition additive manufacturing process," *Journal of Manufacturing Processes*, vol. 29, pp. 149–159, 2017, doi: 10.1016/j.jmapro.2017.07.019.
28. R. Aziz, M. I. Ul Haq, and A. Raina, "Effect of surface texturing on friction behaviour of 3D printed polylactic acid (PLA)," *Polymer Testing*, vol. 85, Art. no. 106434, 2020, doi: 10.1016/j.polymertesting.2020.106434.

Disclaimer/Publisher's Note: The statements, opinions and data contained in all publications are solely those of the individual author(s) and contributor(s) and not of Publisher and/or the editor(s). Publisher and/or the editor(s) disclaim responsibility for any injury to people or property resulting from any ideas, methods, instructions or products referred to in the content.